

Substorm related changes in precipitation in the dayside auroral zone – a multi instrument case study

A. J. Kavanagh^{1,2}, F. Honary¹, I. W. McCrea², E. Donovan³, E. E. Woodfield⁴, J. Manninen⁵, and P. C. Anderson⁶

¹Department of Communication Systems, Lancaster University, Lancaster, UK

²EISCAT Group, Space Science and Technology Dept., Rutherford Appleton Laboratory, Chilton, Didcot, Oxfordshire, UK

³University of Calgary, 2500 University Drive NW, Calgary, Alberta, Canada

⁴Department of Physics and Astronomy, University of Leicester, Leicester, UK

⁵Sodankylä Geophysical Observatory, Tähteläntie 112, FIN-99600 Sodankylä, Finland

⁶Aerospace Corporation, Space and Environmental Technology Center, Los Angeles, USA

Received: 17 October 2001 – Revised: 16 April 2002 – Accepted: 22 April 2002

Abstract. A period (08:10–14:40 MLT, 11 February 1997) of enhanced electron density in the D- and E-regions is investigated using EISCAT, IRIS and other complementary instruments. The precipitation is determined to be due to substorm processes occurring close to magnetic midnight. Energetic electrons drift eastward after substorm injection and precipitate in the morning sector. The precipitation is triggered by small pulses in the solar wind pressure, which drive wave particle interactions. The characteristic energy of precipitation is inferred from drift timing on different L-shells and apparently verified by EISCAT measurements. The IMF influence on the precipitation in the auroral zone is also briefly discussed. A large change in the precipitation spectrum is attributed to increased numbers of ions and much reduced electron fluxes. These are detected by a close passing DMSP satellite. The possibility that these ions are from the low latitude boundary layer (LLBL) is discussed with reference to structured narrow band Pc1 waves observed by a search coil magnetometer, co-located with IRIS. The intensity of the waves grows with increased distance equatorward of the cusp position (determined by both satellite and HF radar), contrary to expectations if the precipitation is linked to the LLBL. It is suggested that the ion precipitation is, instead, due to the recovery phase of a small geomagnetic storm, following on from very active conditions. The movement of absorption in the later stages of the event is compared with observations of the ionospheric convection velocities. A good agreement is found to exist in this time interval suggesting that $\mathbf{E} \times \mathbf{B}$ drift has become the dominant drift mechanism over the gradient-curvature drift separation of the moving absorption patches observed at the beginning of the morning precipitation event.

Key words. Ionosphere (auroral ionosphere; particle precipitation) Magnetospheric physics (storms and substorms)

1 Introduction

The incoherent scatter radar is probably the most powerful tool available for the study of the ionosphere, and during periods of intense precipitation, an estimate of the electron density is possible at heights starting at around 65 km. The greatest limitation of the method is in the narrow beam of the instrument providing only a single time series of height profiles. Similarly the riometer (relative ionospheric opacity meter) is restricted in that it provides indications of the precipitation into the D-region around heights of 90 km but provides no direct measurement of the altitude profiles. Chains of riometers can provide a good indication of the spatial scale and movement of absorption features related to precipitation (Rosen and Winkler, 1970). With the inception of the imaging riometer (Detrick and Rosenberg, 1990) observations of precipitation over a wide field-of-view became possible and combining the observations of the riometer with those of the incoherent scatter radar expands significantly the scope of the two instruments (e.g. Collis and Hargreaves, 1997; Collis et al., 1997).

Precipitation into the high latitude auroral zones is predominantly through scattering of energetic particles from closed field lines, which are then lost into the denser atmosphere. The scattering process is usually due to the growth of wave particle interactions, feeding and extracting energy from the trapped, mirroring particles and altering the pitch angle distribution. These ELF/VLF waves are detected using radio receivers, however ground based magnetometers detect the signature of ULF waves which may play a role in mod-

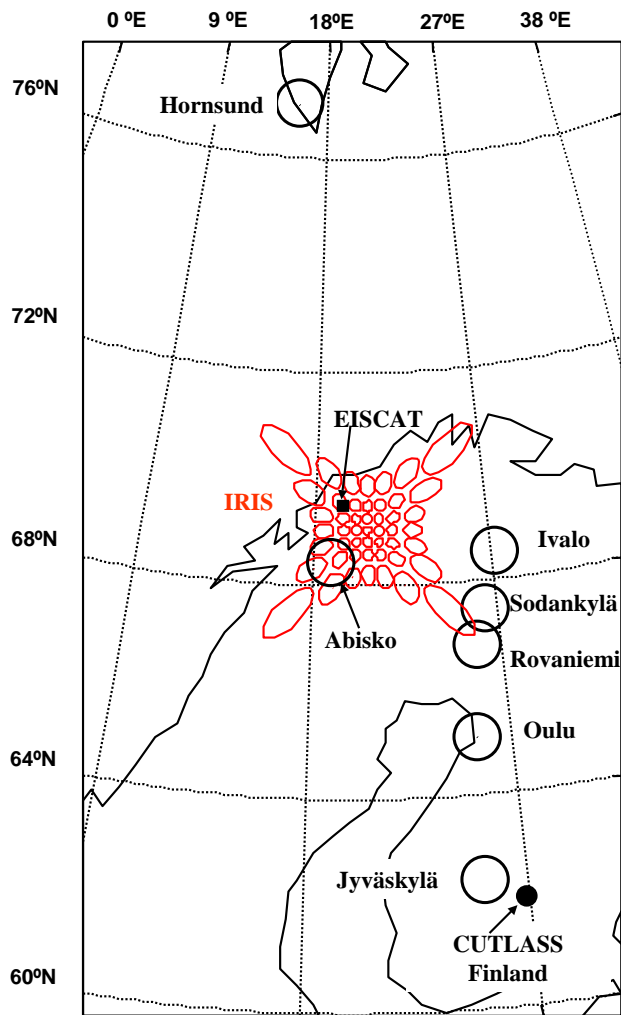


Fig. 1. A map of northern Scandinavia illustrating the positions of some of the instruments used in this study. This includes IRIS, EISCAT, CUTLASS and the SGO riometer chain. The pulsation magnetometer is co-located with IRIS at Kilpisjärvi (69.05° N, 20.79° E).

ulating the VLF wave particle interaction process (Coroniti and Kennel, 1970). The dynamics of the precipitation provide an insight into the solar wind-magnetosphere coupling and interactions on the dayside. An increase in solar wind dynamic pressure can drive precipitation in the auroral zones (Brown et al., 1961) and the location and scale size is dependent on the position of the open-closed field line boundary (Brown, 1978). Nishino et al. (1999) demonstrated that changes in the IMF (interplanetary magnetic field) can also lead to increases in high latitude absorption due to the intensification of field aligned currents close to the location of the cusp. Absorption in the morning sector is a common occurrence (e.g. Hargreaves, 1969; Hargreaves and Berry, 1976). This absorption has been linked to precipitation of eastward drifting electrons, injected on the night side during substorm activity; however some discrepancies between the theory and the observations still arise (Hargreaves and Devlin, 1990).

In this paper we present an example of enhanced lower altitude electron density observed in the morning sector and around magnetic local noon in the auroral zone on the 11 February 1997. This corresponds to slowly varying, but high, HF radio absorption and changing ionospheric flows. The mechanisms of precipitation are discussed with reference to particle injection during substorms and the ensuing gradient-curvature drifts of the energetic electrons.

2 Instrumentation

Throughout the period of interest the mainland UHF European Incoherent Scatter radar (EISCAT) at Tromsø (69.59° N, 19.23° E geographic coordinates) was running the field aligned cp1k programme (Rishbeth and Williams, 1985). The data presented in this paper are from the power profile (scaled to give an estimate of the electron density) and start at an altitude of ~65 km in the D-region ending at ~180 km altitude (lower F-region). A two-minute integration period is used.

The Imaging Riometer for Ionospheric Studies (IRIS) at Kilpisjärvi (69.05° N, 20.79° E, geographic coordinates) has been active since September 1994, operating at 38.2 MHz (Browne et al., 1995). The antenna consists of a 64-element dipole phased array that provides 49 imaging beams over a 240 by 240 km field-of-view. The horizontal beam widths in the D-region are of the order of 20 km near the zenith and all the beams are sampled every second. The beams are numbered from the west to east in seven rows from 1 to 49. The field aligned EISCAT beam intersects with beam 16 of IRIS at 90 km altitude. The riometer operates by monitoring the cosmic radio noise and comparing the received power to a quiet day level when contributions from precipitation are insignificant. These quiet day curves (QDC) are generated through an empirical method, refined at Lancaster University (S. R. Marple, private communication), to account for seasonal variations. Sodankylä Geophysical Observatory operates a chain of broad beam riometers. Each instrument operates at frequencies around 30 MHz, however for this study they have all been corrected for 38.2 MHz using the assumption that the absorption is proportional to the inverse square of the frequency (Hargreaves, 1969). Each riometer uses a theoretical quiet day curve that will produce errors relative to the method for IRIS QDC generation, however with high, slowly varying absorption (such as throughout this event) any differences due to QDC are insignificant.

Figure 1 shows the locations for the riometers used in this study, together with the locations of the EISCAT site at Tromsø and the location of the Finland HF radar of CUTLASS (Cooperative UK Twin Located Auroral Sounding System), part of the Super Dual Auroral Radar Network (SuperDARN) (Greenwald et al., 1995). The radar has 16 beams and was running in standard common mode with 45 km range gates. All beams have a dwell time of 7 s with the scan synchronised to start every 2 min. Not enough ionospheric scatter was present from the Iceland East site

of CUTLASS during this event and so it has been omitted from the study. Three passes of DMSP spacecraft close to EISCAT ($\leq 10^\circ$ longitude away) occurred throughout the event. The DMSP satellites are in sun synchronous orbits at ~ 830 km altitude with ~ 100 min orbital periods. The F10 spacecraft is gradually precessing to later local times at a rate of ~ 15 min/year. The auroral particle sensors (SSJ4) on the DMSP (Defence Meteorological Satellite Programme) spacecraft (F10, F12 and F13) measure precipitating particles in the energy range of 30 eV to 31 keV, in 20 channels each for ions and electrons (Hardy et al., 1984). The higher end of this range overlaps with the lower end of the sensitivity of IRIS, which detects the influence of high-energy electrons (10 s of keV). All magnetic coordinates and L-values discussed in this paper are in the Altitude Adjusted Corrected Geomagnetic coordinate system (Baker and Wing, 1989) using the IGRF-2000 (International Geomagnetic Reference Field) model.

3 Observations

The interval preceding 11 February 1997 was particularly active. A large magnetic cloud had passed the Earth on 10 February and the interplanetary magnetic field (IMF) had been highly variable throughout the preceding week with high solar wind speeds up to ~ 650 km/s at the L1 point. By the time of the event presented here (06:00 to 12:30 UT, 11 February 1997) the wind speed had slowed to around 450 km/s and continued to slow throughout the day reaching a low of 400 km/s by 11:40 UT. Figure 2 shows the northward (B_z) and eastward (B_y) components of the IMF together with the dynamic ion pressure during the event. The data come from the GEOTAIL satellite (Kokobun et al., 1994; Mukai et al., 1994), which was moving duskward in the solar wind at about $10 R_E$. This suggests that the satellite was in the magnetosheath, between the bowshock and the magnetopause. The timing from the magnetopause to the foot of the ionosphere is estimated to be approximately 2 min (Stauning et al., 1995a). Data from the satellite are available from 06:00 UT to 12:00 UT.

Figure 3 shows the time series from three ground-based instruments starting from 06:00 UT (08:10 MLT at EISCAT) on 11 February 1997. The top panel shows raw electron density values between 65 and 180 km measured by the EISCAT radar, uncorrected for the electron to ion temperature ratio. This correction is not expected to be important at E-region heights and below where $T_e \sim T_i$. The center panel contains the cosmic radio noise absorption from beam 16 of IRIS, measured in decibels (dB). The bottom panel is a spectrogram from the search coil magnetometer co-located with IRIS at Kilpisjärvi. The intensity of pulsation is illustrated for frequencies from 0 to 1 Hz (arbitrary units). The EISCAT data shows that a substantial enhancement in electron density occurs from 06:20 UT. This is located in a height band of ~ 83 to 116 km. The density enhancement maximises at $\sim 2.2 \times 10^{11} \text{ m}^{-3}$ and lasts until 06:40 UT. Cosmic radio

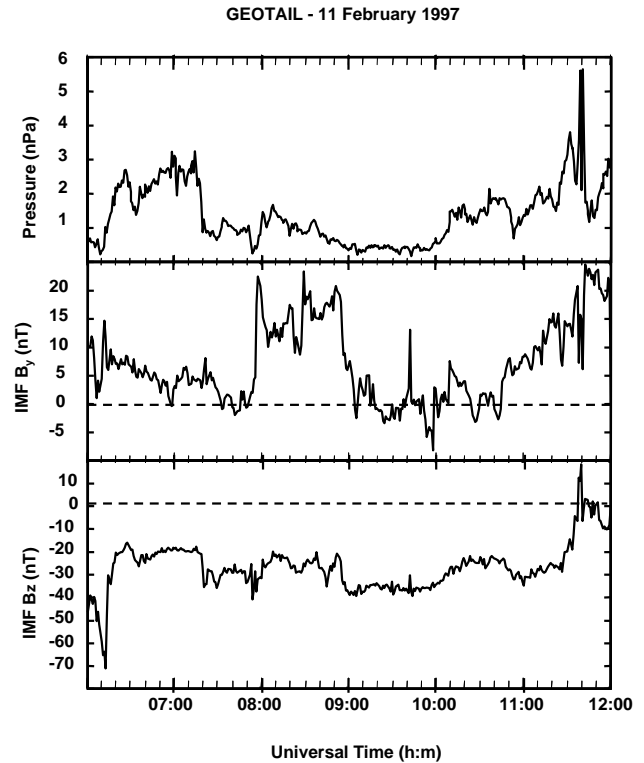


Fig. 2. Solar Wind data taken from the GEOTAIL spacecraft. The satellite was crossing the front of the magnetopause at $10 R_E$ for the duration of this event. The panels illustrate (bottom to top): predominantly negative IMF B_z , positive IMF B_y and the low solar wind dynamic pressure.

noise absorption is approximately proportional to the height-integrated product of the effective collision frequency and the electron density in the D-region; thus there is a sharp 1 dB rise at 06:20 UT. On inspection of the multi-beam data, the northernmost beam of IRIS observes an increase of 1 dB at 06:15 UT, which then expands equatorward, covering the whole field-of-view by 06:50 UT. With the assumed delay time from GEOTAIL the initial increase in absorption corresponds with a small rise (2.4 nPa) in solar wind ion pressure over ~ 15 min.

Figure 4 shows particle flux-energy spectrograms from two DMSP satellites. The top panel displays data from the F13 satellite split into electron and ion fluxes. The satellite crossed the magnetic latitude (Mlat) of EISCAT at 06:33 UT, 10° longitude west of the radar beam and indicated by the solid, vertical black line. The dispersed ion signatures from 06:30 to 06:32 UT indicate that the satellite is on newly opened field lines, moving south to closed field lines. By the time of crossing EISCAT (06:33 UT) there are no ion signatures; there are, however, relatively high fluxes of low-energy electrons and low to medium fluxes of high-energy electrons (> 2.5 keV). The maximum energy deposition height of a 2.5 keV electron is ~ 130 km, suggesting good agreement with the EISCAT data at this time. The high-energy electrons are still detected to ~ 65 Mlat. Figure 3 shows that a second

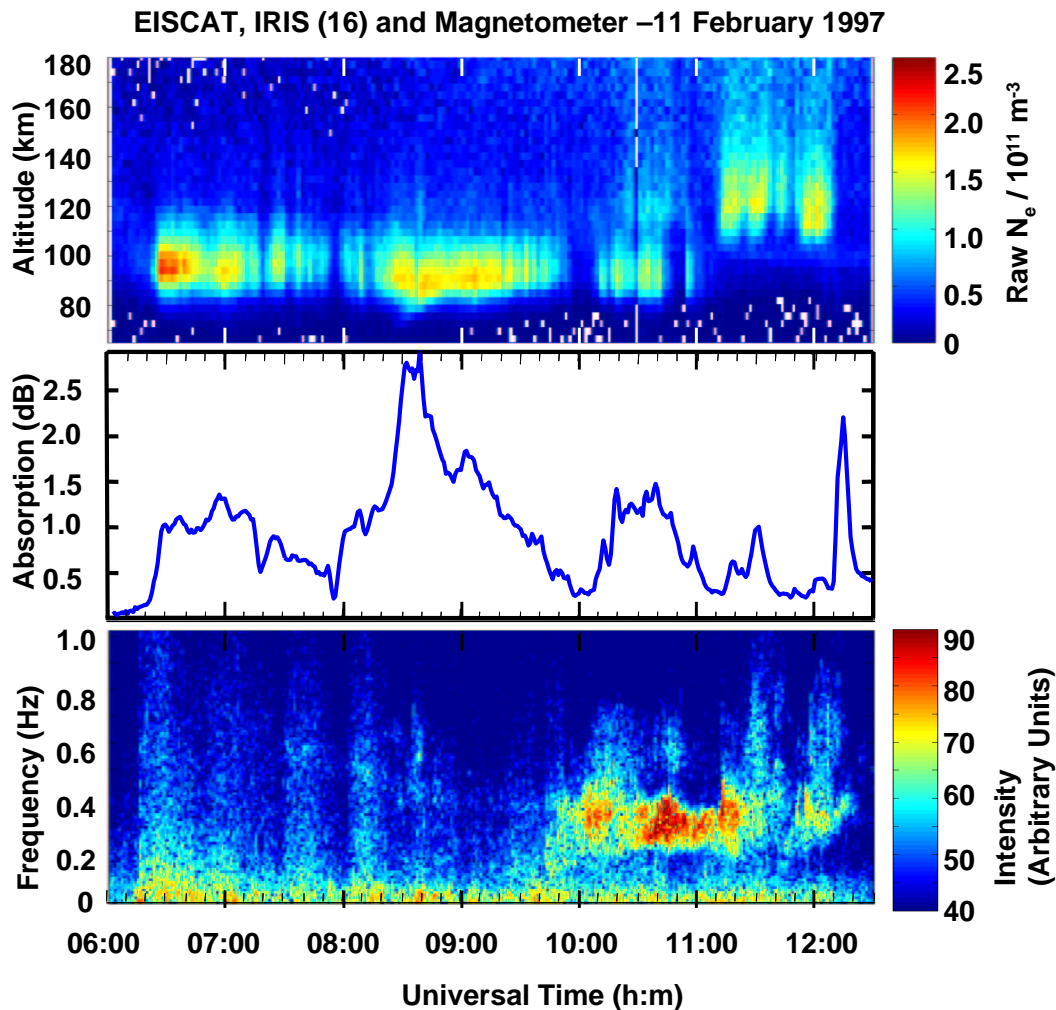


Fig. 3. The top panel shows the EISCAT raw electron density, scaled from the returned power. The middle panel shows the absorption time series from beam 16 of IRIS. The bottom panel is a spectrogram, from the pulsation magnetometer at Kilpisjärvi, with arbitrary units of intensity.

peak in the ionospheric electron density ($\sim 1.7 \times 10^{11} \text{ m}^{-3}$) occurs around 07:00 UT. There appear to be 4 distinct bursts of structured density between 06:00 and 08:00 UT (06:30, 07:00, 07:15 and 07:30 UT) with successively decreasing maxima and narrowing height ranges. The maxima of the enhancements last for 10–15 min. IRIS records matching peaks between 0.6 and 1.3 dB. After 08:00 UT another increase occurs ($1.3 \times 10^{11} \text{ m}^{-3}$) lasting for ~ 10 min. This precedes a large, long duration increase in electron density at 08:15 UT. At 08:35 UT the density increase reaches to a lower altitude of ~ 77 km before gradually rising to the previous altitude limits. This corresponds with high absorption (3 dB). Electron densities remain $> 10^{11} \text{ m}^{-3}$ until 09:50 UT, with an increasing lower altitude limit. This is reflected in the riometer time series as a gradual decrease in absorption. A pass by the F12 satellite at 09:58 UT (5° longitude from EISCAT) coincided with decay in the electron density (data not shown). Low fluxes of energetic electrons were observed

together with softer electron precipitation that deposits in the lower F-region, in good agreement with the EISCAT data. The EISCAT observations can be placed in a spatial context by considering the nearby chain of riometers.

Figure 5 is a stack plot of the riometer data, incorporating the IRIS wide beam. The top panel is from the Hornsund instrument located at the southern tip of Svalbard. The remaining instruments are on the mainland and are ordered in descending magnetic latitude (see Fig. 1). The Y-axis divisions are 0.5 dB. Neither Hornsund (73.8° Mlat) nor Jyväskylä (58.8° Mlat) witness absorption above 0.5 dB from 06:00 to 12:30 UT, placing a definite latitudinal limit to the precipitation. The time lag in the event onset can be seen in the riometer chain. Oulu (61.5° Mlat) does not see increased absorption until 08:00 UT. At this time the riometers from Abisko to Oulu see a rise of at least 2 dB maximising after 08:40 UT. The absorption reaches background levels at Oulu by 10:00 UT.

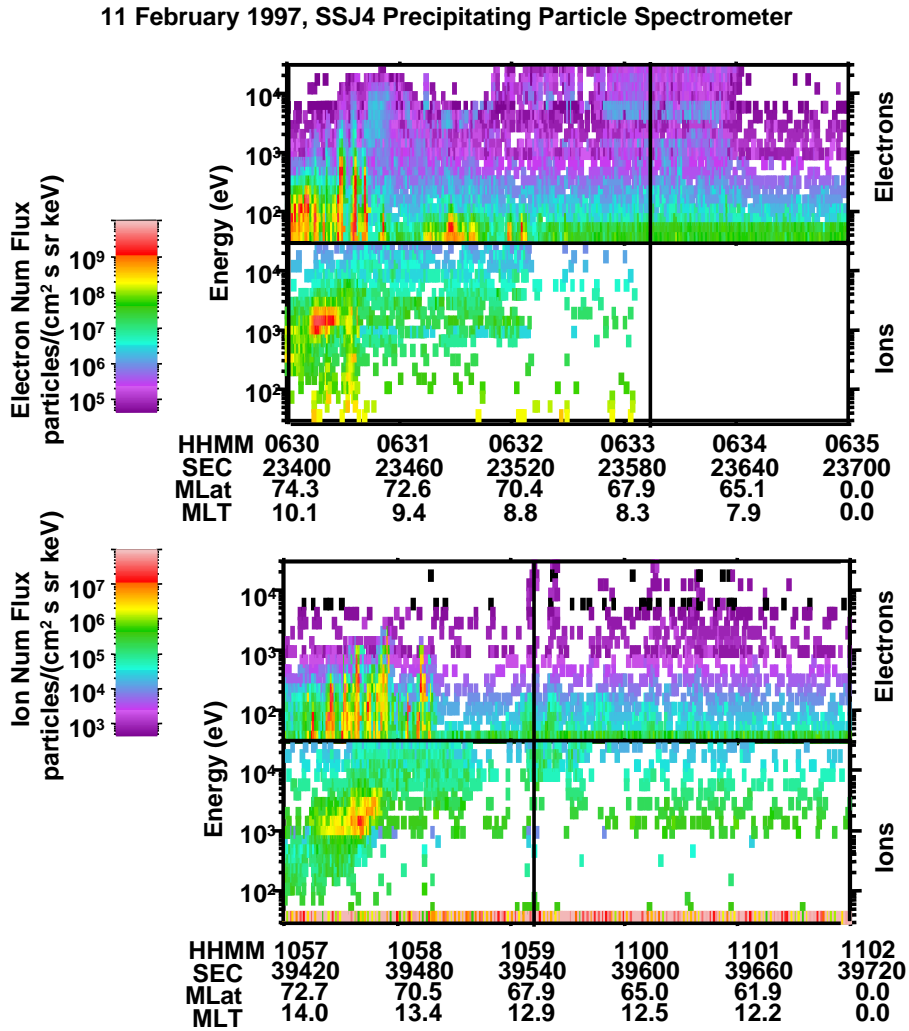


Fig. 4. Two passes from DMSP satellites are shown. The black vertical lines illustrate the times of crossing the magnetic latitude of EISCAT. The top panel is from the F13 spacecraft around 06:30 UT. The bottom panel is a pass by the F10 satellite close to 11:00 UT.

Throughout the precipitation event, the Finnish search-coil magnetometer at Kilpisjärvi observes intense pulsations particularly in the < 0.2 Hz range (Fig. 3, bottom panel). From 06:00–10:00 UT there are low intensity pulsations of < 1 Hz, with a maximum below 0.4 Hz. There is some time coincidence of the bursts of electron density with the pulsations lasting for 10 to 15 min and separated by ~ 10 min intervals. The weakest burst of pulsations coincides with the large increase in absorption at 08:40 UT. After 09:45 UT, there are much more intense, continuous pulsations occurring in the frequency range of 0.2 to 0.6 Hz. This frequency band narrows over the next 90 min. From 10:00 UT, a change in the altitude spread of the electron density occurs (Fig. 3, top panel). Enhancements range from ~ 80 km to 130 km altitude, with lower density values. The absorption peaks at about 1.4 dB due to the extended height range of electron density. The final DMSP pass (Fig. 4, bottom panel) is by the F10 satellite at 10:59 UT (7° longitude away). Once

again there is the dispersed ion signature as the satellite travels equatorward through the cusp. There is a distinct lack of energetic electrons at this time; however, there are fluxes of 10 s of keV ions over a short latitude range. This coincides with the E-region densities observed by EISCAT and the structured Pc1 pulsations recorded by the magnetometer. Although there is evidence of softer electrons, there are also high fluxes of energetic ions (10–30 keV) that could account for the E-region densities. Around 11:00 UT, the ionosphere starts to lift so that by 11:12 UT most of the D-region density has disappeared. Instead there are strong densities ($> 1.5 \times 10^{11} \text{ m}^{-3}$) in the E-region with ‘tails’ extending into the lower F-region. These seem to occur in 4 short and narrowly separated bursts, each lasting 10 to 15 min. The absorption over EISCAT is relatively low, with the exception of a short duration 1 dB spike at 11:30 UT. A sharp cut-off in electron density occurs shortly after 12:10 UT and densities then remain low until late evening. The large spike in the

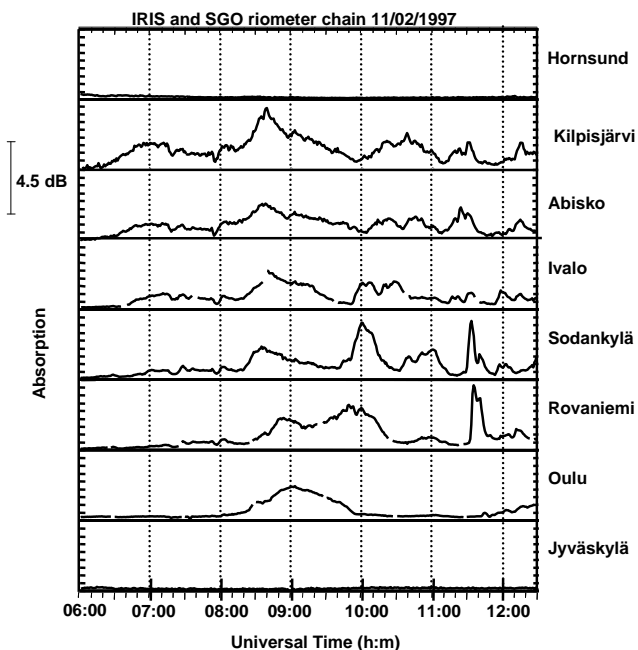


Fig. 5. A stack plot of riometer data comprised of IRIS and the SGO chain. The instruments are ordered by descending magnetic latitude.

absorption data at 12:15 UT is due to a drifting, narrow arc that is partly covered by beam 16 but does not pass through the much narrower beam of EISCAT. At 11:12 UT, the magnetometer observes structured pulsations covering the range of 0.2 to 0.5 Hz with the upper limit gradually rising to 1 Hz and the lower limit increasing to 0.4 Hz over the next 30 min. This structure is repeated at 11:50 UT and coincides with northward turnings of the IMF. The first of these is clear in the data from GEOTAIL (Fig. 2).

The small-scale spatial development of the absorption over EISCAT can be ascertained from the keogram in Fig. 6. The keogram is a slice across the field-of-view at constant geographic longitude (19.2°). The equatorward expansion at 06:15 UT is clear and the large increase at 08:40 UT seems to occur simultaneously in all beams. The northward drift observed by the riometer chain is visible in the keogram after 09:40 UT with the most intense absorption being confined to the south end of the field-of-view, away from EISCAT. A patch of absorption at 11:10 UT drifts poleward and westward with levels exceeding 3 dB. A second patch follows at 11:30 UT, this one extending further north (66.4° Mlat). The arc of absorption at 12:15 UT meanders poleward as well, but as discussed earlier, it does not enter the EISCAT radar beam.

Figure 7 displays the line of sight velocities from beam 5 of the CUTLASS Finland radar that passes over EISCAT. Negative values represent velocities away from the radar site and the dashed horizontal line indicates the latitude of EISCAT. The lack of data from Iceland East means that velocity vectors are not available for 06:00 to 12:30 UT, but beam 5 points approximately meridionally. The scatter is

patchy for much of the event; however, the velocities after 11:00 UT are high (sometimes reaching > 800 m/s) and increase in the westernmost beams. The eastern beams show lower velocities at this latitude, even turning equatorward at the easternmost beam. This indicates that EISCAT is in a region of strong ionospheric return flow as the field lines convect poleward towards the cusp and across the polar cap. Velocities previous to this tend to be low (± 200 m/s) as the direction of flow is most likely perpendicular to the radar line of sight.

Finally, simultaneous night side observations are provided by the CANOPUS (Canadian Auroral Network for the OPEN Program Unified Study) array of instruments. Figure 8 shows the response of several instruments to the varying geomagnetic activity. The top panel displays the magnetic signature at Gillam, filtered for Pi2 pulsations. The central panel shows the latitude integrated (red) and peak (black) intensity observed by the Gillam Meridian Scanning Photometer (MSP) at 557.7 nm. The bottom panel is a stack of riometers from the Churchill line; Churchill, Gillam and Island Lake from top to bottom. Signal amplitude is illustrated rather than absorption. Low activity occurs locally up until 06:10 UT when a large burst of Pi2 occurs, reaching a maximum at 06:20 UT. This corresponds with increased optical activity and a sharp spike in the riometer data indicating energetic precipitation. Magnetic midnight occurs at 06:30 UT at the Gillam site. Activity remains high from 06:00 UT to 10:00 UT with Pi2 fluctuations of ± 20 nT and variable optical signatures in the MSP related to drifting auroral arcs. A second strong burst of activity occurs shortly before 08:00 UT (01:30 MLT) and then again around 09:00 UT (02:30 MLT) and beyond.

4 Discussion

Here we discuss different possibilities for explaining the absorption observed by IRIS related to the enhanced electron densities. Three main areas are addressed: the effect of the solar wind pressure, drifting electrons from substorm injection and time influence of the IMF on changes in precipitation. From these topics, the precipitation on the morning of 11 February 1997 may be characterized as arising from a combination of two distinct geophysical phenomenon; the recovery phase of a small storm and drifting electrons from enhanced nightside activity coupled with solar wind pressure changes. Finally the spatial development of the absorption is considered and compared with ionospheric flows measured by coherent radar. This enables the differentiation of dominating flow regimes at different times during the event.

4.1 Solar wind pressure

The timing of the first increase in absorption coincides with the first rise in solar wind pressure at around 06:20 UT assuming a short delay from the magnetosheath to the ionosphere, and the time structure of the absorption broadly follows the changing pressure. Small changes in the pres-

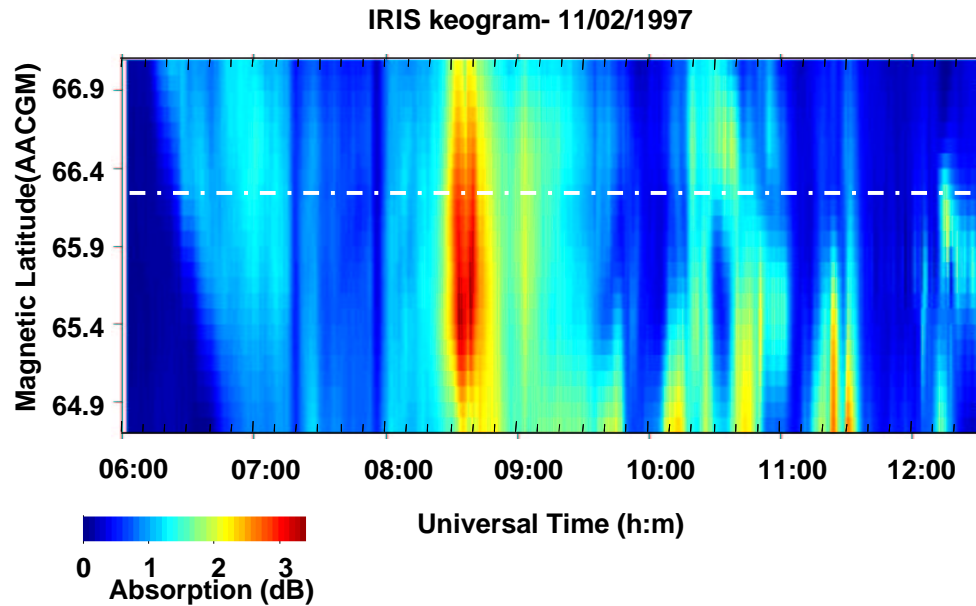


Fig. 6. Keogram taken at constant geographic longitude. The image is a composite from the IRIS beam data and includes beam 16 that overlaps the field aligned EISCAT radar beam in the D-region. The dashed white line indicates the latitude of EISCAT.

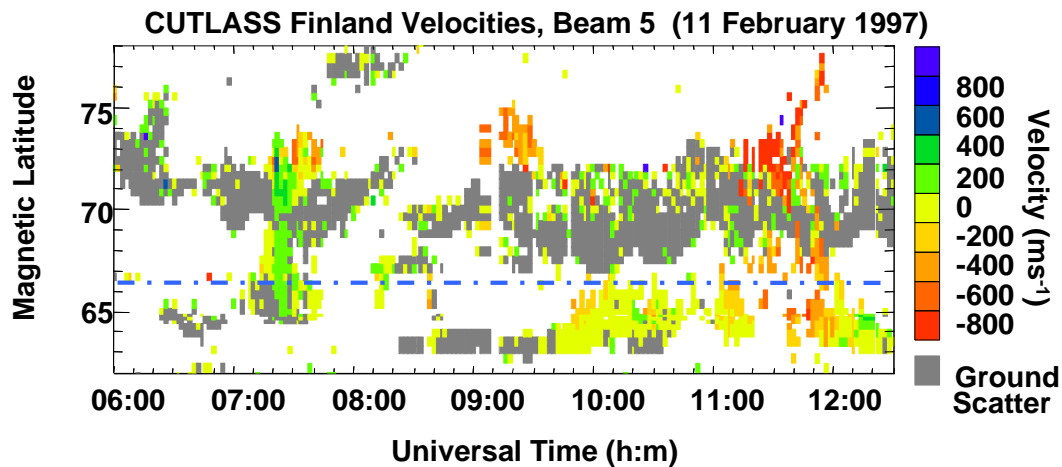


Fig. 7. Line of sight velocities from beam 5 of the CUTLASS Finland HF radar. Negative velocities are away from the radar site (approximately poleward). The radar was operating under normal scanning mode for this period. The horizontal dashed line indicates the latitude of EISCAT. Data from the neighbouring CUTLASS beams show similar features but are not presented.

sure are reflected in changing absorption levels in the riometer. The pressure-absorption relationship breaks down after 08:15 UT (at EISCAT) when the pressure decays to < 1 nPa within 30 min whereas the absorption continues to increase. This is due to a hardening of precipitation, as indicated by the increase in electron density at lower altitudes evident in the EISCAT data. Pressure pulses in the solar wind are well known to produce increases in auroral precipitation (Brown et al., 1961; Brown and Driatsky, 1973) through wave particle interactions in the magnetosphere, leading to enhanced

ionospheric absorption (Perona, 1972). This sudden commencement absorption (SCA) is often associated with poleward moving absorption regions (Brown, 1978); however, in this case the absorption spreads equatorward at onset (Fig. 6). SCAs are usually associated with pressure increases of at least an order of magnitude greater than the values observed during this event. From this it may be surmised that the solar wind pressure is not the sole cause of the elevated electron density observed at EISCAT. The coincidence in the temporal structure of the pressure and the absorption suggests that

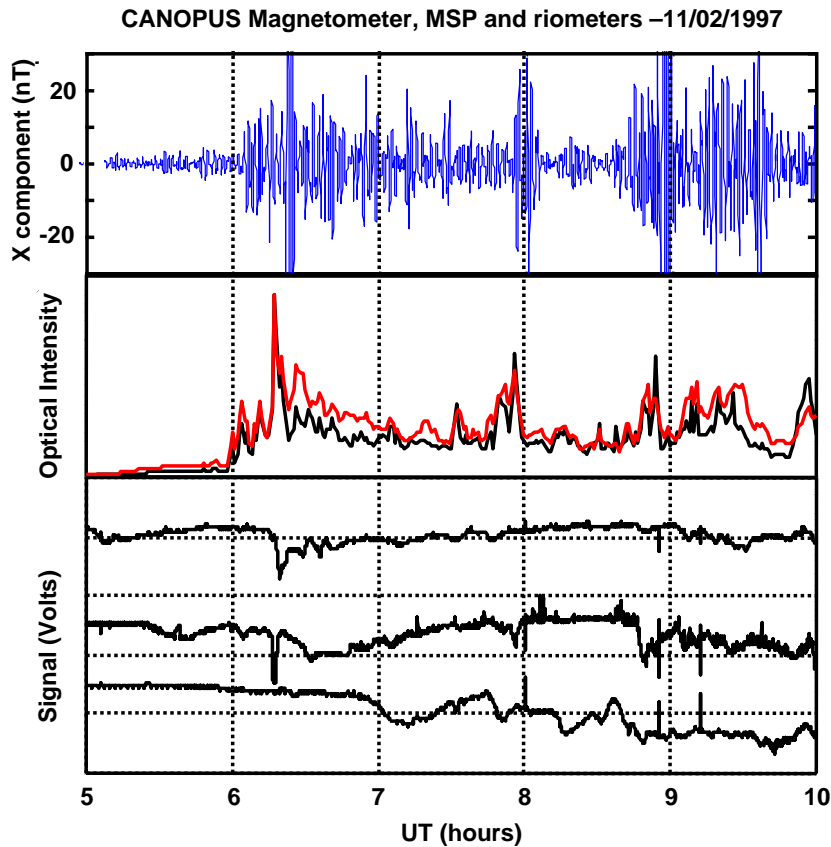


Fig. 8. CANOPUS nightside observations illustrating elevated geomagnetic and auroral activity. The Pi2 filtered magnetic signature at Gillam is shown (top) with latitude-integrated (red) and peak (black) optical intensity at 557.7 nm from a co-located MSP (middle). The bottom panel is a stack plot of riometers from the Churchill line; Churchill, Gillam and Island Lake from top to bottom.

the solar wind plays a role in the precipitation of the electrons in this case; however, similar observations are needed to confirm that this is more than a coincidence. If high fluxes of trapped electrons are present small fluctuations in the magnetic field will encourage the growth of resonant waves. This will lead to pitch angle diffusion amongst the particle population, resulting in scattering into the loss cone and hence precipitation (Schulz and Lanzerotti, 1974). A mechanism by which elevated fluxes of electrons are injected onto the relevant field lines still needs to be identified for this event.

4.2 Substorm drifts

The electron density enhancements from 06:15 UT correspond with bursts of < 0.6 Hz pulsations (Fig. 3). On average, these bursts last for 10 to 15 min with a ~ 10 -min separation suggesting a Pc5 like modulation. Stauning (1998) and Kikachi et al. (1988) observed some slowly varying absorption events to be related to strong pulsations in the Pc4–5 range. Stauning et al. (1995b) and Stauning (1998) describe the theory that absorption in the morning sector displaying this slowly varying nature was related to the drizzle of eastward drifting electrons from substorm activity on the nightside. Those observations were from the Sondre Stromfjord IRIS at 73.5° Mlat. The CANOPUS observations (Fig. 8) confirm that substorm activity was occurring in the Canadian sector at this time. Activity at the Gillam

site started shortly after 05:00 UT. The magnetometer indicates low intensity Pi2 signatures at this time, related to a small brightening in the 557.7 nm emission between 70° and 64° latitude. Major activity begins after 06:00 UT with a large Pi2 signature at 06:20 UT accompanied by a spike in the absorption from the co-located riometer at Gillam. Figure 9 shows the AE index (top panel) and D_{st} index for 11 February 1997. The period of observation at EISCAT is highlighted in red. A sharp increase in the AE index occurs around 05:00 UT followed by a much larger increase occurring after 06:00 UT. This reinforces the CANOPUS observations of the geomagnetic activity.

The timing of the expansion of absorption at onset, across the IRIS field-of-view, gives an estimate of the energy of precipitating electrons if it is assumed that electrons are injected onto all relevant L-shells simultaneously. The IRIS keogram (Fig. 6) illustrates a distinct gradient in the precipitation at event onset. The IGRF-2000 model was used to identify two IRIS beams (beams 2 and 46) that have the same magnetic longitude and to calculate their L-values. During the initial period of activity a time difference of about 25 min was observed between the appearances of absorption features in these two beams.

Assuming constant values for the magnetic field the drift period of a particle can be expressed, following Hargreaves

(1995), as:

$$P = \frac{733}{E} \cdot \frac{1}{R} \cdot \frac{G}{F} \text{ hours} \quad (1)$$

E is the energy of the particle in keV, R is the equatorial distance, in earth radii, and G/F is a function that depends on the mirror point of a particle. Close to the equator $G/F = 1$ and increases to 1.5 for particles mirroring at the poles. It is clear that a particle will take longer to complete an orbit on a lower L -shell than a similar particle at higher L . Particles which mirror at the equator are ignored for the purpose of this calculation since they are less likely to precipitate than those that mirror at the poles. Thus G/F is taken to be 1.5 for the following estimation. It should be noted that particles are injected on the nightside and precipitate after dawn, thus they complete only a fraction of an orbit. For the purpose of this calculation we make the assumption that particle injection occurs around magnetic midnight. This follows the observations of Vagina et al. (1996) using LANL and GOES geosynchronous spacecraft to detect dispersed particle populations and magnetic field dipolarization. These signatures of the injection region occurred between 21:00 and 01:00 MLT with most before but close to midnight. Thus in this case the injection region is chosen to be around 24:00 MLT. Assuming this injection period, a particle that precipitates at 08:20 MLT will have travelled just over 8 h of magnetic local time. Thus a particle precipitating at 06:15 UT will have travelled 35% of its predicted orbital period and a particle precipitating at 06:50 UT will have travelled 38%. Hence, the time separation of precipitation from a single characteristic energy (E) on two field lines (R_1 and R_2) at similar magnetic longitude can be expressed as:

$$T_2 - T_1 = \Delta T = \frac{1099.9}{E} \times \left(\frac{0.38}{R_2} - \frac{0.35}{R_1} \right) \quad (2)$$

Where ΔT defines the time difference of precipitation occurring on field lines R_2 and R_1 . Thus for the two IRIS beams at $L = 6.65$ and $L = 5.62$, $E \approx 37$ keV.

This method assumes that electrons are injected, simultaneously, over the range of $L = 5.62$ to 6.65 . EISCAT shows a maximum of electron density between 85 and 105 km altitude at 06:20 UT, peaking close to 92 km. The maximum ionisation production of a 37 keV electron occurs at an altitude of ~ 90 km (Rees, 1963). Thus EISCAT appears to verify that the drift timing gives a reasonable estimate of the characteristic energy of the electrons responsible for the D-region density enhancements.

Equation (1) indicates that there is an inverse relationship between the period of a gradient-curvature drifting particle and its energy. Thus, as may be expected, for a given L -shell a higher energy particle will drift around the Earth at a higher velocity than a particle of lower energy. This leads to an energy dispersion signature in the particle population that can be observed by satellites (e.g. Vagina et al., 1996). If this is the case then it is reasonable to assume that, at event onset, the electron density enhancements observed at EISCAT will be due to a limited spectrum of precipitating electrons.

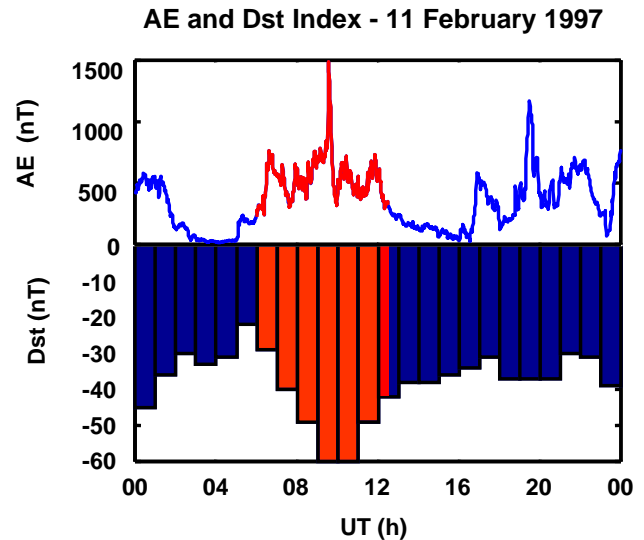


Fig. 9. Hourly D_{st} and the 1 min AE indices for 11 February 1997. The periods in red denote the times of observation at EISCAT. The whole period was relatively active but a minimum in the D_{st} index occurs around 09:00 to 11:00 UT. AE shows an initial sharp increase close to 05:00 UT before a much larger step after 06:00 UT.

This can be tested in two ways; the first is by looking at data obtained from low orbit satellites (such as DMSP), the second method inverts the EISCAT electron density profiles to obtain an estimate of the energy spectrum of precipitation.

Hargreaves and Devlin (1990) used the second approach to study morning sector precipitation during two intervals. In both cases, the events were much earlier in local time; however, the principal of energy dispersion still holds. The conclusions of that study indicate that the maximum electron density occurs a short while after onset and that the spectra tend to be relatively broad. This is not consistent with the theory of drifting electrons that suggests that the maximum occurs at the onset and that the energy spectrum will be narrow due to the energy dispersion of the particle population. The method used in that previous paper has been applied to EISCAT profiles from the current study. A description of the procedure (ZABMOD) can be obtained from the appendix of Hargreaves and Devlin (1990) but, in brief, it is an iterative process that operates between 65 and 110 km altitude with energies from 5.9 to 380.5 keV; an assumption about the background electron density at these heights can be ignored, especially for un-illuminated periods.

Figure 10 shows the results for two electron density profiles close to the onset of the event on the 11 February 1997. There is an initial hardening of the spectrum that occurs over a short time range (~ 10 min). Pure Gradient Curvature drift predicts that the maximum should occur as a sharp onset. It is reasonable to expect that dispersion in the particle energies will result in a changing signature at IRIS/EISCAT as the lower energy electrons arrive at a later time. This appears to occur in the gradual rising of the lower edge in the EISCAT electron density (Fig. 3, top panel) between 07:00 and

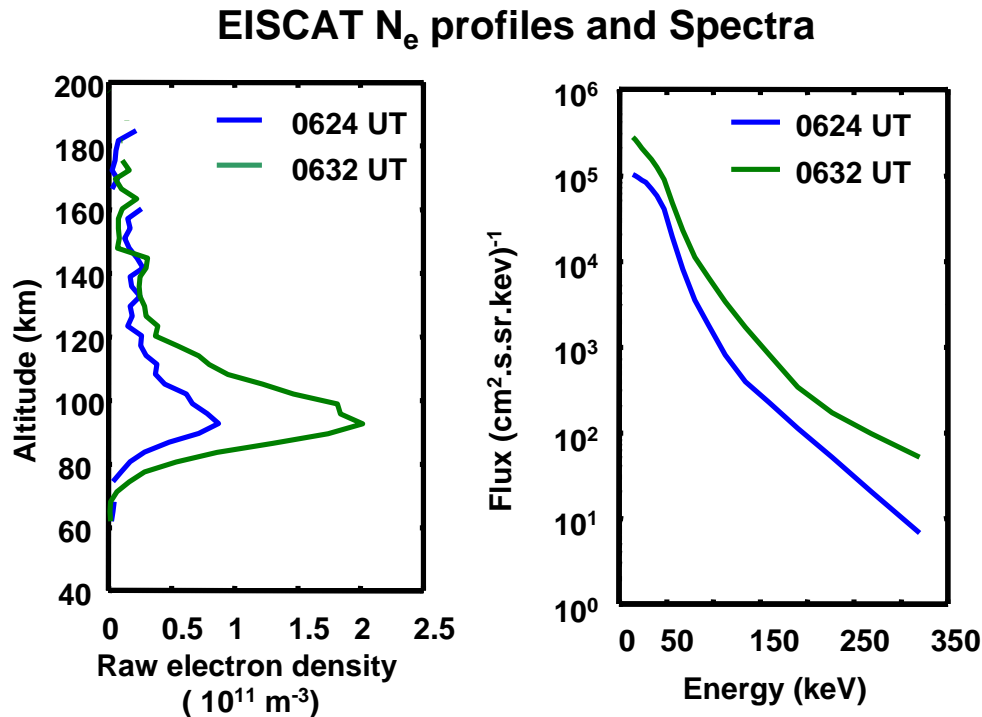


Fig. 10. The first panel contains EISCAT measured electron density profiles for two times close to the onset of the event. The second panel shows the corresponding modelled energy flux spectra, calculated from the profiles using the ZABMOD method. Note the hardening of the spectrum from 06:24 UT to 06:32 UT.

08:00 UT and also after 09:00 UT, though continuing substorm activity observed by CANOPUS suggests that fresh populations are injected at later times. The increased Pi2 signature after 06:15 UT suggests that substorm activity is overhead at the Gillam site (local time = 23:45 MLT). The activity continues throughout the early event with the most intense Pi2 pulsations displaying similar quasi periodicity to the dayside precipitation suggesting a link to the small fluctuations in the solar wind pressure.

The pass of the DMSP F12 satellite at 06:33 UT shows that there were particles of ~ 30 keV present on field lines close to EISCAT. The flux at this energy is approximately $3 \times 10^5 \text{ cm}^{-2} \text{ s}^{-1} \text{ sr}^{-1} \text{ keV}^{-1}$ showing good agreement with the derived spectrum. However the satellite also indicates that there is precipitation of electrons with energies lower than the estimated level. These particles must come from another source to the drifting electrons that produce the D-region density enhancements at EISCAT.

As stated earlier, precipitation of drifting electrons has been reported at the Sondre Stromfjord IRIS (e.g. Stauning et al., 1995b; Stauning, 1998) and also at the Japanese IRIS located at Ny Ålesund on Svalbard (e.g. Nishino et al., 1999), both at higher magnetic latitudes and closer to the polar cap boundary than the present observations. The results presented in this paper support the notion that gradient-curvature drift cannot be the only explanation for the structure and occurrence of morning sector precipitation.

4.3 IMF influences and changes in precipitation spectrum

Nishino et al. (1999) observed a rectified response, during a morning absorption event, to north-south excursions of the IMF. Their observations were from the IRIS at Ny Ålesund ($\sim 76.1^\circ$ Mlat) and they concluded that the rectified response was due to the movement of the convection boundary and intensification of field aligned currents. In the case presented here, the interplanetary magnetic field configuration was predominantly southward and no such response is observed, however a change in precipitation does occur with changing IMF over larger time scales. The point of most intense precipitation (08:40 UT) occurs as the solar wind pressure dies away during a decrease in clock angle, due mostly to a large positive step in B_y . This change in B_y will result in a change in the convection pattern in the ionosphere and so alter the configuration of the geomagnetic field (Cowley et al., 1991; Khan and Cowley, 2001). A change in the latitudinal spread of absorption occurs whilst B_y is positive. The rise in absorption at 08:20 UT, due to the increased lower altitude electron densities, occurs almost simultaneously from Kilpisjärvi to Oulu, although Oulu peaks later. The previous absorption had shown little effect at Oulu ($L = 4.3$). Precipitation continues for a longer duration at this time (~ 90 min) than for the previous bursts in which the electron density decayed within 25 min on average. The distribution of absorption suggests two events occurring simultaneously; the

first a continuation of the drizzle of precipitation confined to higher latitudes, the second a burst of precipitation extending from deeper in the magnetosphere and across a larger range of L-shells. If the magnetosphere changes in a shorter time span than the drift period of a particle, radial diffusion of the particle could occur. Since the dayside magnetic field lines have been skewed due to the change in IMF, B_y , a drifting particle will encounter a local change of field. As the particle moves onto a lower L-shell it will experience acceleration due to the stronger field and shorter field lines. Thus higher energy fluxes are produced at the lower L-shells. With continuing wave particle interaction leading to pitch angle scattering into the loss cone, precipitation of higher energy electrons across a broader range of latitudes will be observed.

An alternative to this mechanism is that substorm injection is occurring across a larger range of L-shells with higher energy particles being injected. The CANOPUS data show that there is increased activity shortly before 08:00 UT. The precipitation is not as enhanced as the onset at 06:00 UT; however, there is a spike in both the optical intensity and in the riometer data, suggesting energetic precipitation. By assuming that maximum activity is occurring around local midnight and that the hardening of the spectrum at EISCAT is due to drifting electrons, it is possible to estimate the characteristic energy. Thus if injection occurs at 07:50 UT and the electrons precipitate at 08:40 UT, we would expect a characteristic energy of ~ 80 keV. This corresponds to a maximum ionisation production height of ~ 86 km which is reasonably consistent with the altitude of peak electron density observed by EISCAT. A combination of these higher energy electrons coupled with radial diffusion could result in the deeper penetration and enlarged latitudinal spread of absorption that occurs at 08:40 UT.

After 10:00 UT (12:10 MLT) changing conditions are reflected both in the electron density profile, which shifts towards a maximum in the E-region, and in the drastic change in the geomagnetic pulsation spectrum (Fig. 3). This change occurs as the instrument location rotates equatorward of the cusp in a region of strong return flow in the ionospheric convection pattern as indicated by the CUTLASS HF radar at Hankasalmi (Fig. 7). This direction of flow also appears in the movement of the absorption region seen in both IRIS and the riometer chain where there is a poleward and westward flow. The DMSP pass at 10:59 UT (Fig. 4, bottom panel) indicates the presence of higher energy ions on field lines close to EISCAT with low energy electrons suggesting that the change in density profile is due to increased ion precipitation rather than electrons. Regions of both high poleward flow and high and variable spectral width in HF radars have been shown to indicate the location of the ionospheric footprint of the cusp (Baker et al., 1995). Both CUTLASS and DMSP observations place the equatorward edge of the low altitude cusp a few degrees north ($\sim 71^\circ$ Mlat) of the EISCAT site. Ion precipitation is common in the cusp and both the Boundary Plasma Sheet (BPS) and Low latitude boundary layer (LLBL) have been observed to contain ions with energies exceeding 30 keV (the upper limit of the DMSP space-

craft) (Lockwood, 1997). It is possible that the ion signatures observed at EISCAT could be related to precipitation from the LLBL or BPS and the energies seem reasonable. The magnetometer shows bands of Pc1 pulsations, which are taken to be signatures of ion-cyclotron waves and lead to scattering of ions into the ionosphere. Narrowband waves in the Pc1 range have been detected close to the equatorward edge of the cusp near to the low-latitude boundary layer (e.g. Dyrud et al., 1997) giving credence to the speculation that the ions observed at EISCAT are related to the LLBL. It is expected that the Pc1 pulsations reach a maximum intensity when the equatorward edge of the cusp is located close to the station; however, in comparing the signature from the magnetometer at Kilpisjärvi (65.8° Mlat) with observations from a similar instrument at Sodankylä (63.9° Mlat) (data not shown), the lower latitude station observes more intense, but similarly structured, pulsations at this time. The distance from EISCAT to the equatorward edge of the cusp casts doubt on this being a reasonable assumption and the likelihood of the precipitation being related to the cusp/LLBL is diminished. The increase in intensification at lower latitudes coincides with increased absorption at those stations related to increased electron density. Figure 6 shows that the south end of the IRIS array observes higher absorption than the region around EISCAT. Thus the precipitation of energetic ions is maximising deep in the magnetosphere, at low L-shells. The changes in the structure of the Pc1 signature occur at similar times to two northward excursions of the IMF. Ion precipitation was occurring before this, during the narrow band pulsations. The change in IMF may influence a change in the wave structure but appears to have little effect on the ion precipitation. The Pc1 waves do indicate that there has been a growth in electromagnetic ion-cyclotron (EMIC) waves in the magnetosphere close to about $L = 4.5$ (Mauk and McPherron, 1980; Anderson et al., 1992a; Anderson et al., 1992b). These result in pitch angle scattering of energetic ring current ions, which then precipitate (Gonzales et al., 1994). The EMIC wave growth can be attributed to the interaction of cold plasma with hot ions, as the plasmasphere enlarges and mixes with the ring current (Cornwall et al., 1970; Cornwall, 1978). The ring current ions have been accelerated, either through injection from the tail during the ongoing substorm activity (Arnoldy and Chan, 1969) or via the transport of plasma sheet particles by enhanced convection electric field (Lyons and Schulz, 1989). Since this event occurs after a distinctly active period, it is reasonable to expect the radiation belts to be increased with high fluxes of energetic particles. This theory is reinforced by the D_{st} index (Fig. 9) which shows a minimum of -60 nT occurring between 09:00 and 11:00 UT before increasing as in the recovery phase of a small to moderate geomagnetic storm.

4.4 Ionospheric flows

Low velocities (< 200 m/s) were observed by CUTLASS (Fig. 7) after onset (06:15 UT), most likely due to a predominantly zonal drift with small meridional movement. These

observations are contrary to the movement of absorption observed by IRIS, which displays a distinct equatorward motion after 06:00 UT. From 11:00 UT there is a definite poleward and westward flow of the intense absorption patches to the south end of the riometer field-of-view (Fig. 6). Estimates of the poleward velocities have been made for these patches both through comparisons of time series from consecutive IRIS beams and through the movement of steep absorption gradients in the IRIS images/keogram. Previous studies have shown the drift velocity of absorption patches to be consistent with the $\mathbf{E} \times \mathbf{B}$ drift (Nielsen and Honary, 2000). The current estimates were compared with the flow observed by CUTLASS in the region of high return ionospheric flow. The absorption appears to drift with velocities of ~ 650 m/s from 11:00 to 11:20 UT after which there is a general increase to ~ 900 m/s. The radar backscatter is patchy at this time but several of the radar beams (0 to 11) cut across IRIS providing a good indication of the flows. Only data from beam 5 has been displayed since this is the beam that encompasses the EISCAT beam; however, data from neighbouring beams show that there are similar velocity fields across the IRIS field-of-view. The CUTLASS line of sight velocities pre 11:30 UT, at the latitudes of IRIS, are generally < 600 m/s away from the radar. Post 11:30 UT there is a general increase with some scatter suggesting flows > 800 m/s. These rough calculations suggest good agreement between the movement of the F-region irregularities and the absorption patches in the E- and D-regions. It is therefore reasonable to suggest that the dominant drift mechanism for the precipitating particles at this time is the $\mathbf{E} \times \mathbf{B}$ drift, as opposed to gradient-curvature drift apparently observed at event onset (06:15 UT). If the absorption at the south end of the array is also due to ion precipitation into the E-region, then the tendency to drift as the $\mathbf{E} \times \mathbf{B}$ velocity seems reasonable. Past studies have established that the flow in the E-region is often similar to that in the F-region (Nielsen and Schlegel, 1985). The possibility exists that the scatter observed by CUTLASS could come from the E-region irregularities that compose the electron density enhancements (Milan et al., 2001). An investigation of the elevation angle of the returned HF beam suggests that this is not the case, with angles of $> 21^\circ$ for most of the scatter in the nearer range gates. The E-region densities have well defined ‘tails’ extending into the F-region and so the radar scatter could originate from irregularities in these ‘tails’.

5 Summary and conclusions

A case study is presented of varying precipitation in the morning sector and across noon during an active period on 11 February 1997. The observations were made using an imaging riometer (IRIS) and a nearby incoherent scatter radar (EISCAT) together with a chain of wide beam riometers and two pulsation magnetometers, in conjunction with satellite and HF radar measurements. Through nightside observation, provided by the CANOPUS array of instruments

(including a meridian scanning photometer, magnetometers and riometers) the precipitating electrons have been linked to substorm injection and subsequent gradient-curvature drift. With this assumption, the time separation of absorption increases across the IRIS field-of-view has been used to provide an estimate of the characteristic energy of precipitation (37 keV). This is due to a lag in the drift time of particles on lower L-shells. Observations of electron density from EISCAT suggest that the energy estimate is reasonable. However it is found that gradient-curvature drift alone cannot account for the spectrum of precipitation at EISCAT. The time evolution of the spectrum indicates that softer precipitation was occurring before the higher energy particles, indicative of some other factor affecting the precipitation. A controlling influence from the solar wind has been identified in the form of small-scale pressure changes at the magnetopause, leading to increases in pitch angle scattering in an already unstable energetic population of electrons.

A small increase in particle penetration into the ionosphere has been discussed in relation to increased radial diffusion producing higher energy electrons at lower L-shells. This assumption is based on a dramatic change in the geomagnetic field orientation, transmitted from the IMF, and near simultaneous increase in precipitation. This precipitation leads to enhanced absorption in the nearby riometers and is coupled with the more energetic particles being injected at the nightside. The electron precipitation then decreases, at the same time as an increase in ion fluxes, the latter being identified in data from the over flight of DMSP F10. The possibility that the ions arise from the LLBL or BPS has been dismissed, not only because of the relatively large distance to the cusp but also because Pc1 waves are observed to increase in intensity at lower L-shells. Instead it has been suggested that the ion precipitation is due to a growth in EMIC waves resulting in pitch angle scattering of ions into the loss cone. This has been attributed to an interaction between an enlarged plasmasphere and energetic ring current during the recovery phase of a small to moderate geomagnetic storm. At this later time ($> 13:00$ MLT), IRIS was located under a region of strong poleward convection. The flows observed by CUTLASS at this time were found to be comparable with the movement of strong absorption patches as derived from the IRIS keogram unlike at the start of the precipitation ($\sim 08:30$ MLT). This suggests that $\mathbf{E} \times \mathbf{B}$ drift is governing the precipitating particles at this time rather than L-shell separation of the drifting electrons as at event onset (06:15 UT to 06:50 UT).

This study illustrates how a selection of different instruments can be used to describe better the processes involved in a single, local event and how they can differentiate between overlapping features, both in space and time. The combination of ground-based instruments located in the day and night sectors shows how localized events can be placed in a global context. The precipitation events observed on 11 February 1997 have been inferred to arise from two distinct causes; recovery phase of a small storm and drifting electrons from enhanced nightside activity coupled with solar wind activity. Although drifting electron precipitation has

been observed by the imaging riometer at higher magnetic latitudes, it is believed that these are the first reported observations made using the IRIS at Kilpisjärvi. As far as the authors are aware, it is also the first time that precipitating particle energies have been estimated solely using IRIS.

Acknowledgements. The Imaging Riometer for Ionospheric Studies (IRIS) is operated by the Department of Communications Systems at Lancaster University (UK), funded as a UK National Facility by the Particle Physics and Astronomy Research Council (PPARC) in collaboration with the Sodankylä Geophysical Observatory. EISCAT is an International Association supported by Finland (SA), France (CNRS), the Federal Republic of Germany (MPG), Japan (NIPR), Norway (NFR), Sweden (NFR) and the United Kingdom (PPARC). The CUTLASS HF radars are deployed and operated by the University of Leicester, and are jointly funded by PPARC, the Swedish Institute for Space Physics, Uppsala, and the Finnish Meteorological Institute, Helsinki. CANOPUS operations are funded by the Canadian Space Agency. The CANOPUS riometer data has been baselined by E. Spanswick. Data from the Finnish chain of riometers was provided by Sodankylä Geophysical University, an independent national institute of the University of Oulu. Thanks to Dr. Tilmann Bösinger of the Space Research Group of the University of Oulu, who kindly provided the search coil magnetometer data. GEOTAIL magnetic field data and plasma data were provided by S. Kokubun and T. Mukai through DARTS at the Institute of Space and Astronautical Science (ISAS) in Japan. Thanks to Dr. J.K. Hargreaves who provided useful insights and spectra from the ZABMOD process. AJK is indebted to both PPARC and the Rutherford Appleton Laboratories for a CASE research studentship. AJK is also grateful to M.J. Kosch and A. Grocott for helpful comments and suggestion on this paper.

The Editor in Chief thanks T. Rosenberg and another referee for their help in evaluating this paper.

References

- Anderson, B. J., Erlandson, R. E., and Zanetti, L. J.: A statistical study of Pc 1–2 magnetic pulsations in the equatorial magnetosphere 1. Equatorial occurrence distribution, *J. Geophys. Res.*, **97**, 3075–3088, 1992a.
- Anderson, B. J., Erlandson, R. E., and Zanetti, L. J.: A statistical study of Pc 1–2 magnetic pulsations in the equatorial magnetosphere 2. Wave properties, *J. Geophys. Res.*, **97**, 3089–3101, 1992b.
- Arnoldy, R. L. and Chan, K. W.: Particle substorms observed at the geostationary orbit, *J. Geophys. Res.*, **74**, 5019–5028, 1969.
- Baker, K. B. and Wing, S.: A new magnetic coordinate system for conjugate studies at high latitudes, *J. Geophys. Res.*, **94**, 9139–9143, 1989.
- Baker, K. B., Dudeney, J. R., Greenwald, R. A., Pinnock, M., Newell, P. T., Rodger, A. S., Mattin, N., and Meng, C.-I.: HF radar signatures of the cusp and low-latitude boundary layer, *J. Geophys. Res.*, **100**, 7671–7695, 1995.
- Brown, R. R.: On the Poleward Expansion of Ionospheric Absorption Regions Triggered by Sudden Commencement of Geomagnetic Storms, *J. Geophys. Res.*, **83**, 1169–1171, 1978.
- Brown, R. R. and Driatsky, V. M.: Further Studies of Ionospheric and Geomagnetic Effects of Sudden Impulses, *Planet. Space Sci.*, **21**, 1931–1935, 1973.
- Brown, R. R., Hartz, T. R., Landmark, B., Leinbach, H., and Orner, J.: Large-Scale Electron Bombardment of the Atmosphere at the Sudden Commencement of a Geomagnetic Storm, *J. Geophys. Res.*, **66**, 1035–1041, 1961.
- Browne, S., Hargreaves, J. K., and Honary, B.: An Imaging Riometer for Ionospheric Studies, *Elect. Comm. Eng. J.*, **7**, 209–217, 1995.
- Collis, P. N. and Hargreaves, J. K.: Co-ordinated Studies Using Imaging Riometer and Incoherent Scatter Radar, *J. Atmos. Sol. Terr. Phys.*, **59**, 873–890, 1997.
- Collis, P. N., Hargreaves, J. K., Howarth, W. G., and White, G. P.: Joint Imaging Riometer – Incoherent Scatter Radar Observations: A Four-dimensional Perspective on Energetic Particle Input to the Auroral Mesosphere, *Adv. Space Res.*, **20**, 1165–1168, 1997.
- Cornwall, J. M.: On the role of charge exchange in generating unstable waves in the ring current, *J. Geophys. Res.*, **87**, 1188–1196, 1978.
- Cornwall, J. M., Coroniti, F. V., and Thorne, R. M.: Turbulent loss of ring current protons, *J. Geophys. Res.*, **75**, 4699–4709, 1970.
- Coroniti, F. V. and Kennel, C. F.: Electron precipitation pulsations, *J. Geophys. Res.*, **75**, 1279–1289, 1970.
- Cowley, S. W. H., Morelli, J. P., and Lockwood, M.: Dependence of convective flows and particle precipitation in the high latitude ionosphere on the X and Z-components of the interplanetary magnetic field, *J. Geophys. Res.*, **96**, 5557–5564, 1991.
- Detrick, D. L. and Rosenberg, T. J.: A Phased-Array Radiowave Imager for Studies of Cosmic Noise Absorption, *Radio Science*, **25**, 325–338, 1990.
- Dyrud, L. P., Engebretson, M. J., Posh, J. L., Hughes, W. J., Fukunishi, H., Arnoldy, R. L., Newell, P. T., and Horne, R. B.: Ground observations and possible source regions of two types of Pc1–2 micropulsations at very high latitudes, *J. Geophys. Res.*, **102**, 27 011–27 027, 1997.
- Gonzales, W. D., Joselyn, J. A., Kamide, Y., Kroehl, H. W., Rostoker, G., Tsurutani, B. T., and Vasyliunas, V. M.: What is a geomagnetic storm?, *J. Geophys. Res.*, **99**, 5771–5792, 1994.
- Greenwald, R. A., Baker, K. B., Dudeney, J. R., Pinnock, M., Jones, T. B., Thomas, E. C., Villain, J. P., Cerisier, J. C., Senior, C., Hanuise, C., Hunsucker, R. D., Sofko, G., Koehler, J., Nielsen, E., Pallinen, R., Walker, A. D. M., Sato, N., and Yamagishi, H.: DARN/SuperDARN: A global view of the dynamics of the high-latitude convection, *Space Sci. Rev.*, **71**, 761–796, 1995.
- Hardy, D. A., Yeh, H. C., Schmitt, L. K., Schumaker, T. L., Gussenhoven, M. S., Huber, A., Marshall, F. J., and Pantazis, J.: Precipitating electron and ion detectors (SSJ/4) on the block 5D/Flights 6–10 DMSP satellites: Calibration and data presentation, *Tech. Rep. AFGL-TR-84–0317*, Air Force Geophys. Lab., Hanscom Air Force Base, Mass., 1984.
- Hargreaves, J. K.: Auroral Absorption of HF Radio Waves in the Ionosphere: A Review of Results from the First Decade of Riometry, *Proceedings of the IEEE*, **57**, 1348–1373, 1969.
- Hargreaves, J. K.: The Solar-Terrestrial Environment, Cambridge University Press, 1995.
- Hargreaves, J. K. and Berry, M. G.: The eastward movement of the structure of auroral radio absorption events in the morning sector, *Ann. Geophysicae*, **32**, 401–406, 1976.
- Hargreaves, J. K. and Devlin, T.: Morning Sector electron precipitation events observed by incoherent scatter radar, *J. Atmos. Terr. Phys.*, **52**, 193–203, 1990.
- Khan, H. and Cowley, S. W. H.: Effect of the IMF B_y component on the ionospheric flow overhead at EISCAT: observations and

- theory, *Ann. Geophysicae*, 18, 1503–1522, 2001.
- Kikuchi, T., Yamagishi, H., and Sato, N.: Eastward propagation of Pc4–5 range pulsations in the morning sector observed with scanning narrow beam riometer at $L = 6.1$, *J. Geophys. Res. Lett.*, 15, 168–171, 1988.
- Kokubun, S., Yamamoto, T., Acuna, M. H., Hayashi, K., Shiokawa, K., and Kawano, H.: The Geotail Magnetic Field Experiment, *J. Geomag. Geoelectr.*, 46, 7–21, 1994.
- Lockwood, M.: Relationship of dayside auroral precipitations to the open-closed separatrix and the pattern of convective flow, *J. Geophys. Res.*, 102, 17 475–17 487, 1997.
- Lyons, L. R. and Schulz, M.: Access of energetic particles to storm time ring current through enhanced radial diffusion, *J. Geophys. Res.*, 94, 5491–5496, 1989.
- Mauk, B. H. and McPherron, R. L.: An experimental test of the ionocyclotron instability within the Earth's magnetosphere, *Phys. Fluids*, 23, 2111–2127, 1980.
- Milan, S. E., Lester, M., Sato, N., and Takizawa, H.: On the altitude dependence of the spectral characteristics of decametre-wavelength E-region backscatter and the relationship with optical auroral forms, *Ann. Geophysicae*, 19, 205–217, 2001.
- Mukai, T., Machida, S., Saito, Y., Hirahara, M., Terasawa, T., Kaya, N., Obara, T., Ejiri, M., and Nishida, A.: The low energy particle (LEP) experiment onboard the Geotail satellite, *J. Geomag. Geoelectr.*, 46, 669–692, 1994.
- Nielsen, E. and Honary, F.: Observations of Ionospheric Flows and Particle Precipitation Following a Sudden Commencement, *Ann. Geophysicae*, 18, 908–917, 2000.
- Nielsen, E. and Schlegel, K.: Coherent radar Doppler measurements and their relationship to the ionospheric electron drift velocity, *J. Geophys. Res.*, 90, 3498–3504, 1985.
- Nishino, M., Nishitani, N., Sato, N., Yamagishi, H., Lester, M., and Holtet, J. A.: A Rectified Response of Daytime Radio Wave Absorption to Southward and Northward Excursions During Northward Interplanetary Magnetic Field: A Case Study, *Advances in Polar Upper Atmosphere Research.*, 13, 139–153, 1999.
- Perona, G. E.: Theory on the Precipitation of Magnetospheric Electrons at the Time of a Sudden Commencement, *J. Geophys. Res.*, 77, 101–111, 1972.
- Rees, M. H.: Auroral ionisation and excitation by incident energetic electrons, *Planet. Space Sci.*, 11, 1209–1218, 1963.
- Rishbeth, H. and Williams P. J. S.: The EISCAT ionospheric radar: the system and its early results, *Q. J. R. Astr. Soc.*, 26, 478–512, 1985.
- Rosen, L. H. and Winckler, J. R.: Evidence for the large scale azimuthal drift of electron precipitation during magnetospheric substorms, *J. Geophys. Res.*, 75, 5576–5581, 1970.
- Schulz, M. and Lanzerotti, L. J.: Particle Diffusion in the Radiation Belts, Springer-Verlag, 1974.
- Stauning, P.: Ionospheric radio wave absorption processes in the dayside polar cap boundary regions, in: Polar cap boundary phenomena, (Eds) Moen, J., Egeland, A., and Lockwood, M., Kluwer Academic Publishers, pp. 233–254, 1998.
- Stauning, P., Claur, C. R., Rosenberg, T. J., Friis-Christensen, E., and Sitar, R.: Observations of solar-wind-driven progression of interplanetary magnetic field B_y -related dayside ionospheric disturbances, *J. Geophys. Res.*, 100, 7567–7585, 1995a.
- Stauning, P., Yamagishi, H., Nishino, M., and Rosenberg, T. J.: Dynamics of Cusp-Latitude Absorption Events Observed by Imaging Riometers, *J. Geomag. Geoelectr.*, 47, 823–845, 1995b.
- Vagina, L. I., Sergeev, V. A., Baker D. N., and Singer, H. J.: Use of mid-latitude magnetic data for modelling and diagnostics of magnetospheric substorms, *Adv. Space Res.*, 18, 229–232, 1996.